Gravitational effects on liquefaction systems for Lunar and Mars exploration

R. Balasubramaniam[1,2], A. Kashani[3], R. Grotenrath[2], W. Johnson[2]

1 Case Western Reserve University, Cleveland, Ohio

2 NASA Glenn Research Center, Cleveland, Ohio

3 NASA Ames Research Center, Moffett Field, California

Abstract

There is interest at NASA, other space agencies, and industry, in the liquefaction of fluids produced through in-situ processes on the surfaces of the Moon and Mars. A multi-center team at NASA recently considered multiple different refrigeration cycles and refrigeration integration methodologies and how these might fit into early liquefaction plants for NASA's exploration initiatives. The rate of liquefaction for these initiatives is quite slow in comparison to large scale terrestrial applications. These studies concluded that, for both structural and heat spreading reasons, integrating the refrigeration tubing on the surface of the storage tank wall is an attractive path to pursue in the near term. In order to develop a technology development path and inform investors, it was desired to investigate the sensitivity of gravity of the processes involved.

An analysis of the condensation processes within the tank is performed. The objective is to determine the sensitivity of liquefaction to gravitational effects. The heat transfer mechanisms include forced convection heat removal to the refrigeration system (or cryocooler), conduction through the tank wall heat exchanger, and convection and condensation on the inner tank wall. Gravity affects the liquefaction process via condensate liquid drainage, natural convection in the ullage, and the shape of the liquid-vapor interface within the tank. Analysis of these mechanisms shows that while there is some sensitivity to gravitational level in general, within the bounds of current interest (rate of liquefaction appropriate to Lunar and Martian applications, and cooling capacity of the cryocooler), this sensitivity of liquefaction to gravity is quite small. Thus, system level testing on the Earth should suffice for the performance prediction and demonstration of liquefaction operations as applicable to Lunar and Martian applications.

1. Introduction

NASA has been developing technology to enable mass production of propellants on the surface of the Moon and Mars for nearly thirty years [1]. Recently, it has been looking at the integration of In-Situ Resource Utilization (ISRU) and propulsion systems in its system architectures [2]. Studies generally point out that due to the large mass of ascent vehicles, large quantities of oxygen and propellant (for example methane for the Mars Ascent Vehicle) are required and it is more efficient to produce them on the planetary surface rather than carry them from the Earth. The ISRU processes typically produce the fluids in gaseous form. The propellants, however, are stored as cryogenic liquids because of the several hundred-fold increase in propellant density afforded compared with storage as a vapor. Therefore, liquefaction of the propellant vapors is an important and integral part of ISRU.

In Ref [2], five different liquefaction technologies for oxygen were analyzed for comparison -- Tube-on-tank (also known as Broad Area Cooling), Tube-in-tank (also known as Integrated Refrigeration and Storage), In-line liquefaction, Linde Cycle, and Conduction based liquefaction. The following assumptions were common to the various liquefaction systems: pure oxygen feed with a flow rate of 2.2 kg/hr at a temperature of 273.15 K, and a liquefaction pressure of 101.3 kPa. The total heat removal rate is 247 W at a liquid temperature of 90.2 K and includes both the sensible and latent heat of the oxygen. The insulation warm boundary temperature was assumed to be 273.15 K and the radiator temperature was assumed to be 260 K that are somewhat conservative and representative of a worst-case Mars environment. From the results of the evaluation as well as other considerations (see Ref [2] for details), the tube-on-tank liquefaction system was chosen for further development. This supports a 10,000 kg per year propellant production rate.

In this paper, a liquefaction analysis is performed for the tube-on-tank liquefaction or the broad area cooling (BAC) system. However, many of the basic fluid phenomena being assessed are similar to other applications. Figure 1 shows a picture of the Prototype cryogenic liquid tank fabricated at NASA GRC for liquefaction testing of oxygen.

Figure 1: Prototype Test Tank for oxygen before and after insulation installation.

The tank is made of aluminum and is designed for a pressure of 345 kPa (50 psia). The nominal diameter of the tank is 1.25 m and the height is 1.96 m. The tank is insulated by a blanket of Multi-Layer Insulation (MLI). The internal volume of the tank is 2.14 m^3. The tank has 8 cooling tubes alternatively stitch welded to it along the tank wall and two manifold sections at the top and bottom for single inputs/outputs to a cryocooler. The tank has structural attachment points at both the top and the bottom of the tank to allow for proper handling, attachment to vacuum chamber lids, and installation in various desired test configurations. A single instrumentation and fluid feedthrough is present at the top of the tank.

A cryocooler loop provides at least 150 W of cooling to the tank wall at nominally 90 K by circulating cold gaseous neon through the cooling tubes. Gaseous oxygen nominally at room temperature is fed into the tank from a pure oxygen source via the vent line for liquefying. The flow rates of gaseous oxygen and the flow of neon are monitored. The tank pressure, the liquid fill level, temperature sensors along a central rake inserted from the tank top, and external tank wall temperatures at selected locations are measured. Oxygen liquefaction testing is expected to be performed in the near future.

The objective of this paper is to analyze the liquefaction of oxygen in the storage tank when broad area cooling is employed. The sensitivity of the liquefaction process to the different levels of gravity on Earth, Moon and Mars are determined and compared.

2. Analysis

2.1 Model assumptions

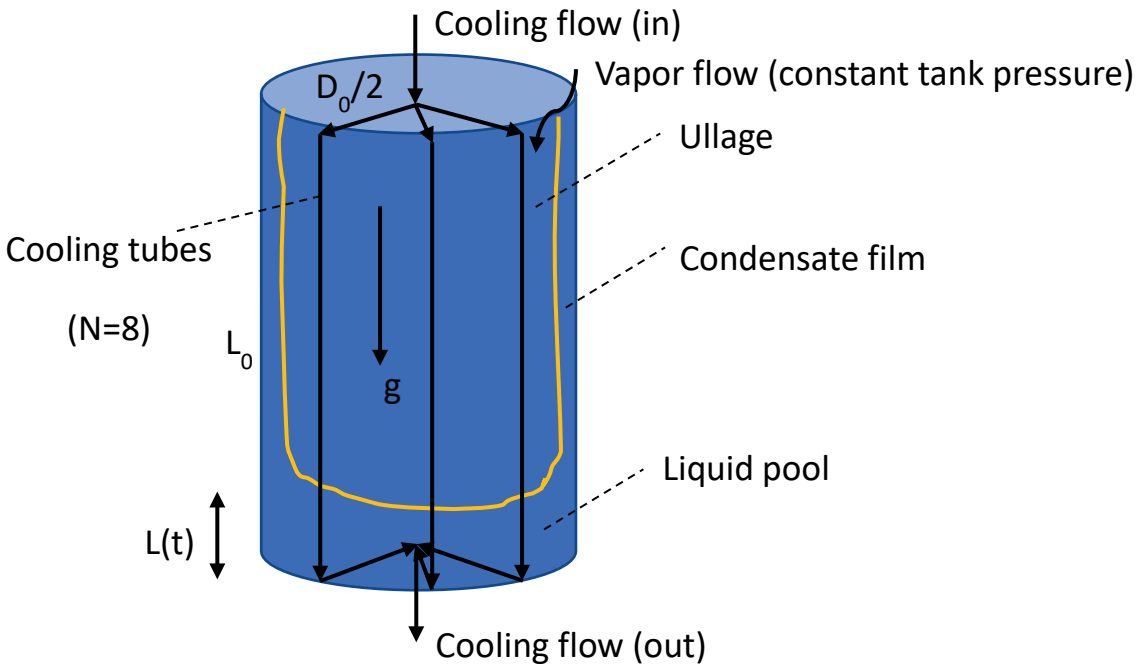

Figure 2: Schematic of the liquefaction tank modeled as being cylindrical.

Figure 2 shows a sketch of the liquefaction process within the storage tank. The tank is assumed to be cylindrical with a flat lid that is maintained at a constant pressure by a flow of gaseous oxygen into it. Cold neon gas flows in eight cooling tubes attached to the outside of the tank wall. It is assumed that the

neon flow is from the top to the bottom as shown in Figure 2. The temperature of the neon is less than the saturation temperature of the gaseous oxygen at the prevailing tank pressure. Thus, oxygen condenses at the tank wall, flows down along the curved surface, and accumulates is a liquid pool at the bottom of the tank. Oxygen also condenses on the upper dome of the tank, that is modeled as a flat lid here for simplicity, and drips onto the liquid pool as droplets.

Gravity affects the condensation process in the tank in several ways. First, the driving force for drainage of the condensation film along the vertical walls is altered. As gravity is reduced, the drainage is slower, and the condensate film is thicker. Second, a significant amount of natural convection is expected to be present in the superheated vapor in the ullage, where the temperature will be in the range from 90 K (saturation temperature of oxygen at 1 atm pressure) to the ambient temperature (~300 K) at which the gaseous oxygen is injected into the tank. The natural convection flow will lead to significant mixing and alter the stratification of the gas in the ullage. This flow (that typically scales as $g^{1/4}$) will be somewhat reduced at the gravity levels on the Moon (1.62 m/s^2, 0.166 times the Earth gravity, approximately 1/6) and Mars (3.96 m/ s^2, 0.377 times the earth gravity, approximately 1/3), but since it typically scales as $g^{1/4}$, the flow reduction will not be severe compared with what happens under Earth's gravity. Third, gravity affects the shape of the liquid-vapor interface. The shape is controlled by the Bond number which is a dimensionless parameter that compares the effects of gravity to the effects of surface tension. When the Bond number is small, the interface shape is spherical and determined by surface tension forces. For partial gravity conditions (such as on the Moon and Mars) and large tank size, the Bond number will be large, and the interface shape will be similar to that seen on Earth. Lastly, the hydrostatic pressure in the tank is determined by gravity. However, the ratio of the pressure change in the liquid is small compared with the tank pressure and is approximately 0.2 for a full tank under normal gravity; in partial gravity, the pressure change in the liquid is reduced and this ratio will be lower.

The following assumptions are made in the analysis so that it can be simplified while retaining the essential physics.

1. It is assumed that the tank pressure is constant. Therefore, as the oxygen vapor condenses into a liquid, a suitable flow of gaseous oxygen into the tank needs to be maintained.

2. It is assumed that the heat transfer within the tank and the neon cooling tubes are at a quasi-steady state, wherein the only time dependence is via the height L(t) of the liquid pool. This is justified because it can be shown that with the available cooling the liquefaction time to fill the tank is on the order of a few months; flow and heat transport time scales within the tank are much smaller than this.

3. It is assumed that condensation on the vertical (cylindrical) tank walls can be modeled by the Nusselt film condensation analysis with extensions incorporated to it by the analysis of Minkowycz and Sparrow [3]. Condensation underneath the tank lid is modeled using the results from the "dripping" condensation analysis of Gerstman and Griffith [4].

4. It is further assumed that there is negligible condensation that takes place at the surface of the liquid pool. This is justified because the condensation film is typically quite small compared with the liquid

pool height L(t), and therefore the temperature gradient in the film region is much larger (orders of magnitude) than that in the liquid pool.

5. The flow of neon in the cooling tubes is assumed to be from the top to the bottom in Figure 2. Thus, the incoming neon is cold at the top of the lid, picks up heat from the tank as it flows in the tubes, and leaves from the bottom of the tank where its temperature will be higher. The neon flow is assumed to be turbulent and the standard Dittus-Boelter correlations is used to calculate the heat transfer coefficient from the walls of the cooling tube to the neon gas. The effects of gravity on the heat transfer to the neon gas within the cooling tubes is assumed to be negligible. This is justified because the Richardson number (Gr/Re^2) that compares the effects of gravity and forced convection for the neon flow is approximately 0.2 in Earth's gravity and smaller under partial gravity. It is assumed that there is negligible resistance to the heat transfer due to conduction in the tube wall (the tube is made of aluminum), as well as any thermal contact resistance between the tank wall and the tube (the tubes are welded to the tank wall). As shown later, the liquefaction rate is limited by the cooling capacity of the neon flow and not by the condensation heat transfer occurring within the tank. Therefore, any additional resistance to the heat transfer outside the tank will further diminish the liquefaction rate as well as the importance of the condensation heat transfer in determining it.

6. Subcooling of the liquid pool by the neon flow over portions of the tank wall below the liquid pool surface is not considered in the model. In reality, the neon flow will remove some heat from the liquid pool that must be transferred to it (at steady state) from the warm ullage.

7. The tank wall temperature is assumed to be uniform in the azimuthal direction at a given tank height. Likewise, the tube wall temperature is assumed to be constant along the periphery of the tube at all locations at a given tank height. The tank wall temperature depends only on the vertical location on the cylindrical surface, and only on the radial location on the lid. Thermal modeling [5] for brassboard tests performed with liquid nitrogen on a similar tank that has a comparable size supports this assumption.

8. The heat leak into the tank from the surroundings through the MLI is assumed to be negligible.

2.2 Heat transfer coefficients

The heat transfer coefficients on the vertical wall can be obtained from the analysis performed by Sparrow and Eckert [6] who extended the original analysis of Nusselt (1916) that only considered simple force and energy balances within the condensate film. Sparrow and Eckert's analysis for a vertical plate includes the coupling of liquid and vapor flow and heat transfer and considers the superheating of the vapor as well as the influence of non-condensable gases in the vapor, if any. For a pure vapor and a thin condensate film thickness, the numerically computed results are well approximated by the following expression for the local and average heat transfer coefficient over the length of the plate.

$$h_x = \left[\frac{\rho_l g(\rho_l-\rho_v)\tilde{h}_{fg}k_l^3}{4\mu_l x(T_{sat}-T_w)}\right]^{1/4},\ h = 0.943\left[\frac{\rho_l g(\rho_l-\rho_v)\tilde{h}_{fg}k_l^3}{\mu_l L_0(T_{sat}-T_w)}\right]^{1/4},\ \tilde{h}_{fg} = h_{fg}\left(1+\frac{C_{p,v}(T_v-T_{sat})}{h_{fg}}\right) \quad (1)$$

where h_x is the local heat transfer coefficient at a location x from the leading edge of the plate, h is the average heat transfer coefficient over the plate of length L_0, ρ_l and ρ_v are the density of the liquid and vapor, h_{fg} is the latent heat of vaporization, μ_l and k_l are the viscosity and thermal

conductivity of the liquid, $C_{p,v}$ is the specific heat of the vapor, g is the acceleration due to gravity, T_{sat} is the saturation temperature of the liquid/vapor at the prevailing tank pressure, T_w is the temperature of the tank wall, and T_v is the temperature of the vapor.

The heat transfer coefficient for condensation underneath the lid at the top of the tank can be obtained from the analysis performed by Gerstmann and Griffith [5]. They predicted the average rate of heat transfer by calculating the shape of the liquid-vapor interface assuming quasi-steady behavior due to a bounded and fully established Taylor instability. Basically, drops of the condensed liquid form at the crests of the unstable liquid-vapor interface in a spatially periodic manner and fall from the surface. The heat transfer coefficient averaged over the wavelength λ ($\lambda \sim l_c$ is of the order of the capillary length $\approx 1mm$ in 1g) of the instability is

$$h = 0.69\frac{k_l}{l_c}Ra^{0.2}, \quad Ra = \frac{\rho_l \sigma h_{fg} l_c}{k_l \mu_l (T_{sat} - T_w)}, \quad l_c = \left(\frac{\sigma}{g(\rho_l - \rho_v)}\right)^{1/2} \tag{2}$$

where l_c is the capillary length, σ is the liquid/vapor surface tension and Ra is a parameter defined by Gerstmann and Griffith (note that Ra is not to be confused with the Rayleigh number that is defined for natural convection flows).

The heat transfer coefficient h_{tube} for the neon flow in the cooling tubes is calculated using the Dittus-Boelter correlation for turbulent flow as

$$h_{tube} = 0.023\frac{k_c}{d_{tube}}Re^{0.8}Pr^{0.3} \tag{3}$$

where k_c and Pr are the thermal conductivity and Prandtl number of neon, Re is the Reynolds number for the neon flow, and $d_{tube}$is the diameter of the cooling tube.

2.3 Energy balances

The energy balance for the flow of neon in each cooling tube can be written as

$$\dot{m}C_p\frac{dT}{ds} = \pi D_{tube} h_{tube}(T_w - T) \tag{4}$$

where T is the temperature of neon, $\dot{m}$ is its mass flow rate, C_p is its specific heat, and s is the arc length along the cooling tube from the inlet. The energy transferred to the tank wall from condensation inside the tank is picked up by neon flow in all the cooling tubes. The energy balance at the tank wall can be written as

$$N[\pi D_{tube} h_{tube}(T_w - T)] = \pi D_0 q_w, \quad q_w = h\,(T_{sat} - T_w) \tag{5}$$

where N is the number of cooling tubes on the tank external surface, D_0 is the tank diameter, and q_w is the heat flux on the tank wall from condensation on the inside surface of the tank.

The boundary condition for the inlet temperature (T_{in}) for neon is

$$T = T_{in}\ at\ s = 0 \tag{6}$$

3. Results

3.1 Heat transfer coefficient estimates

Before presenting the numerical results for the neon and tank wall temperatures as a function of the location on the tank, the magnitude of the heat transfer coefficients in Eqs (1) to (3) are estimated first. The following values for the various parameters are used: N = 8, $\dot{m}$ = 2 g/s (per tube), D_{tube}= 12.7 mm, T_{in} = 80 K, T_{sat} = 90 K, D_0 = 1.25 m, L_0 = 1.96 m. To estimate the condensation heat transfer coefficients, it is assumed that $\Delta T = T_{sat} - T_w = 1$°C.

Table 1: Estimated heat transfer coefficients with $T_{sat} - T_w = 1$°C

	h (W/(m²K))		
	1 g (Earth)	1/3 g (Mars)	1/6 g (Moon)
Nusselt film	2479	1884	1584
Gerstmann model	3971	2559	1939
Neon flow in cooling tube	77	77	77

Table 1 shows that the estimated condensation heat transfer coefficients are O(10^3) W/(m^{2}K)) for 1 g as well as partial gravity on Mars and the Moon, while the heat transfer coefficient for the neon flow is 77 W/(m^{2}K)) and does not depend on the gravity level. Multiplying the h values with the surface area of the cylindrical surface and the lid, the total heat released by condensation can be estimated to be in the range 15 - 24 kW. The heat picked up by the neon flow, however, will not be anywhere near this value and is expected to be in the range 150 to 200 W, with the maximum value limited by the cooling capacity of the cryocooler employed. Therefore, this disparity suggests that $\Delta T = 1$°C used to estimate the condensation heat transfer coefficients is not correct, and in reality $\Delta T \ll 1$°C such that the total heat released by condensation is equal to that transferred to the neon flow. Practically, the entire tank wall can be anticipated to be isothermal at the saturation temperature T_{sat} of oxygen. A curious fact that can be surmised from the heat transfer coefficient and the small condensate film temperature drop in the estimation given above is that the rate of liquefaction is limited by the cooling capacity of the cryocooler and not by the heat transfer characteristics of the condensation processes within the tank, under normal as well as partial gravity levels.

Estimates for various dimensionless parameters are given below for Earth's gravity (note that $\Delta T = 1$°C is used to estimate condensate film parameters).

(i) Condensate film Reynolds number: $Re_f = \frac{4\,h\Delta T\,L_0}{\mu_l\,h_{fgeff}} = 240$, which is well below the transition to turbulence film Reynolds number of 1800.

(ii) Ra defined by Gerstmann and Griffith: $Ra \approx 10^8$ (note that Ra defined by Gerstmann and Griffith is different from and not to be confused with the Rayleigh number defined for natural convection flows).

(iii) Reynolds number for the neon flow: $Re = 16700$, which is larger than the transition to turbulent flow Re of 2300.

3.2 Heat transfer calculations

Equations (4), (5) and (6) are solved numerically starting from the center of the tank-top lid (at arc length $s = 0$, where the neon flow enters the cooling tubes) to the vertical location of the top of the liquid pool in the tank. Note that the location $s = D_0/2$ (the circumference of the top lid) is a singular location geometrically, since it can be considered a part of both the flat tank lid and the cylindrical tank wall. Since the heat transfer coefficients on these two surfaces are given by different expressions (Eq(1) and Eq(2)) and have different numerical values (see Table 1), for the same condensation heat flux, the calculated temperatures T_w at $s = D_0/2$ for the two surfaces will be different and $T_w(s)$ will be discontinuous at $s = D_0/2$. As an example, actual calculations in 1g show that on the tank lid, $T_w(0) = 89.9995$°C and $T_w(D_0/2) = 89.9998$°C, while $T_w(D_0/2) = 90$°C on the vertical tank wall. Thus, the magnitude of the temperature discontinuity is very small and practically negligible. Nevertheless, to avoid the discontinuity, the following ad-hoc approach is used – the vertical wall calculations start from $s = D_0/2 + s_0$, and s_0 is such that $\{T_w(D_0/2 + s_0)\}_{vertical\ wall} = \{T_w(D_0/2)\}_{lid}$. Also, the vertical wall temperature is assumed isothermal between $s = D_0/2$ and $D_0/2 + s_0$. For the example given above, s_0 is computed to be 0.21 *mm*. This approach is used in all the results reported in this paper. Note that the neon temperature is not affected and is continuous at $s = D_0/2$.

Figure 3 shows the calculated temperature distribution for the neon flow (blue curve) and the tank wall (green curve) plotted against the arc length from the center of the tank lid to the bottom of the tank vertical wall. The dotted black lines on the x-axis at $s = 0.625$ m and $s = 2.585$ m denote the edge of the tank lid and the vertical location of the tank bottom, respectively. The calculated temperatures for 1g, 1/3 g and 1/6 g are almost identical and differ by less than approximately 0.5 *mK*. The tank wall temperature is very close to the oxygen saturation temperature T_{sat} = 90 K. The neon temperature rises from its inlet temperature of 80 K to nearly 90 K at the exit at the bottom of the tank.

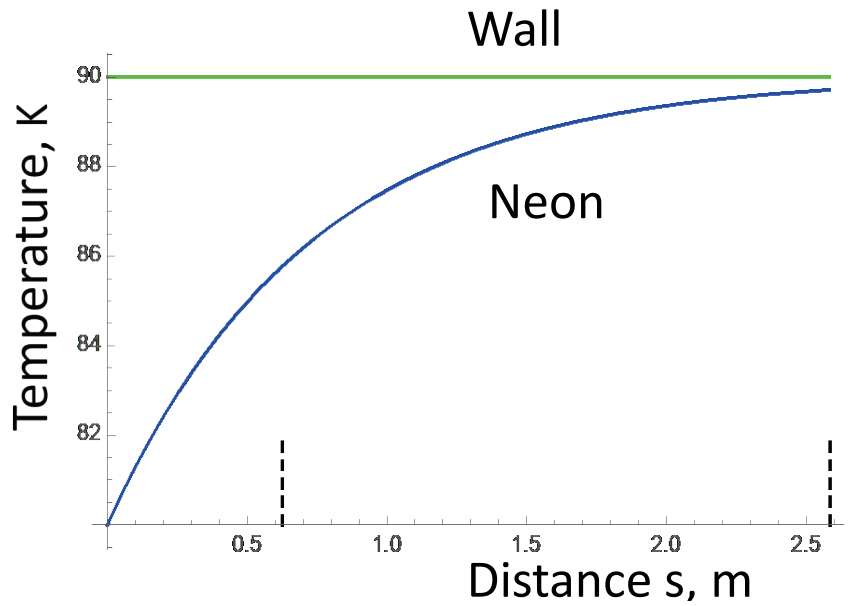

Figure 3: Temperature variation on the tank wall (green curve) and in the neon flow (blue curve). s is the arc-length along the neon flow direction, which is in the radial direction from s = 0 to 0.625 m (on the tank lid) and in the vertical direction from s = 0.625 to 2.585 m (the two dotted black lines in the x-axis).

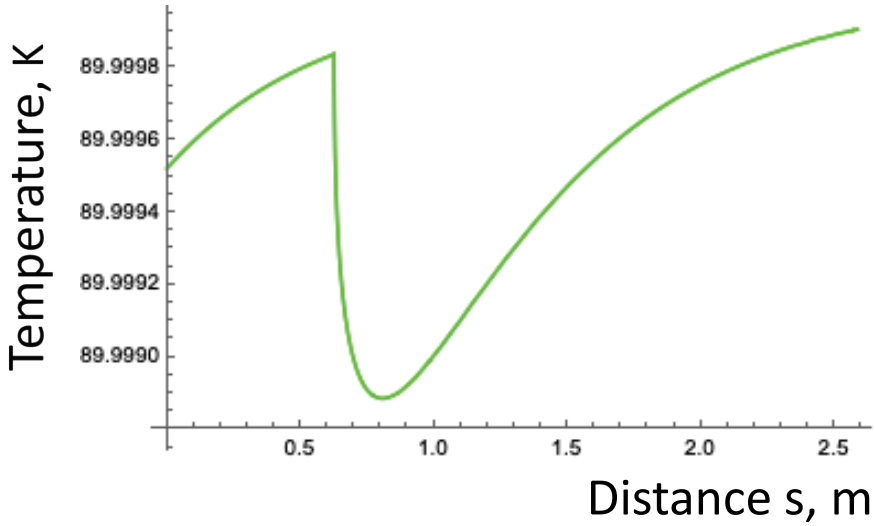

Figure 4: Tank wall temperature variation on an expanded scale

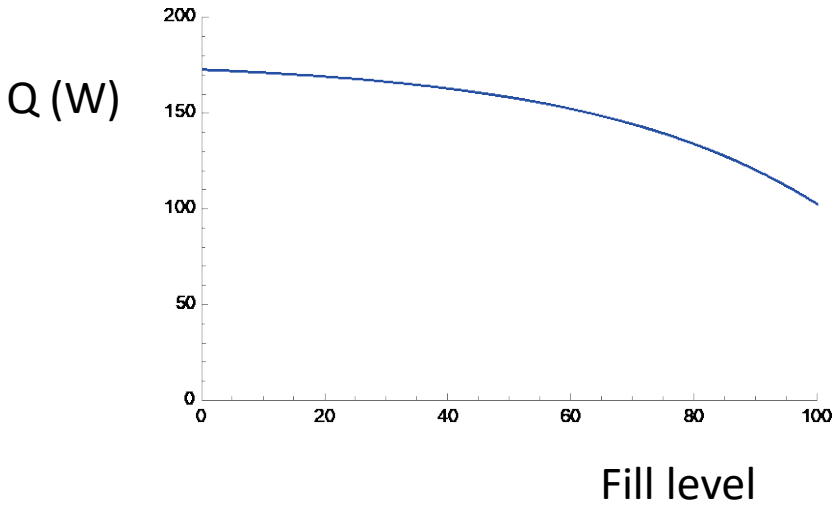

Figure 5: Heat removed from the tank versus fill level.

Table 2: Calculated quantities for the condensate film

	1 g (Earth)	1/3 g (Mars)	1/6 g (Moon)
Average ΔT film (mK)	0.53	0.76	0.96
Average film thickness (μm)	9.2	13.2	16.6
Latent heat Q (W) (0% fill)	173	173	173

Figure 4 shows the tank wall temperature distribution on an expanded scale. The temperature variation is within 1 *mK*. This figure also illustrates the ad-hoc approach mentioned earlier that has been used to make the tank wall temperature continuous near s = 0.625 *m*. Immediately downstream of this location, the condensate film thickness starts to grow and results in a decrease in the tank wall temperature, so that the temperature drop over the film is adequate to transfer the requisite heat flux to the neon flow. Eventually, the tank wall temperature rises again because the neon gets warmer and the heat transfer to it is diminished.

Table 2 shows the results for the average temperature drop and average film thickness in the condensate film on the vertical tank wall, and the latent heat released that is transferred to the neon

flow, for gravity levels on Earth, Mars, and Moon when the tank fill level is zero. The temperature drop in the condensate film is less than 1 mK for the gravity levels considered. The average film thickness is of the order of 10 μm. Figure 5 shows the heat transferred to the neon flow from the top of the lid to the location of the liquid pool in the tank (i.e., the latent heat removed from the tank), as a function of the tank fill level. The heat removed ranges from 173 W when the tank is empty to 103 W when the tank in nearly full (103 W is the heat transferred to the neon flow from the tank lid; also 3 W is transferred to the neon flow from the tank bottom that is not included in Q in Table 2). Figure 5 can also be used to estimate the heat removal from the liquid pool by the neon flow. At 50% fill, the liquid heat removal is approximately 17 W (including the heat removed from the tank bottom).

The heat transfer coefficients and the film Reynolds number that were estimated using $\Delta T = 1$°C can now be revisited using the calculated results. For 1 g, the average heat transfer coefficient from the Gerstmann and Griffith model for the top lid is 24153 W/(m^{2}K), and that in the Nusselt condensate film is 17117 W/(m^{2}K). The film Reynolds number based on the average heat transfer coefficient and average temperature difference in the Nusselt condensate film computes to $Re_f = 0.87$.

4. Discussion

The model pursued here has shown that the condensation of oxygen vapor in the tank is controlled by the rate of heat removed by the neon flow in the cooling tubes, which is ultimately limited by the cooling capacity of the cryocooler employed. While the model is simplistic and does not consider effects such as contact resistance between the tank wall and the cooling tubes, flow due to natural convection in the ullage space and the liquid, and azimuthal temperature variations on the tank wall, it nevertheless shows that for gravity levels on Earth, Mars and the Moon, the heat transfer coefficients due to condensation in the tank far exceeds that due to the turbulent flow of neon within the cooling tubes. Therefore, the tank wall is practically isothermal with its temperature nearly equal to the saturation temperature of oxygen at the prevailing pressure. Under these conditions, the effects of gravity on the heat removal rate and thus the rate of liquefaction is negligible. One can generalize and surmise that (i) any convection inside the tank which typically tends to increase the rate of heat transfer and the value of the heat transfer coefficient or (ii) effects such as contact resistance that tend to diminish the rate of heat transfer to the neon flow, would magnify the importance of the condensation heat transfer coefficient within the tank relative to the heat transfer coefficient external to the tank for heat removal. Thus, the dynamics of the condensation process within the tank and how it is affected by gravity will take an even lesser role in the overall liquefaction process.

On the other hand, effects that tend to decrease the rate of condensation must be considered in judging the design of the liquefaction system. Two well-known effects that tend to diminish the condensation rate are interfacial resistance due to kinetic effects, and the presence of non-condensable gases in the vapor [3]. Interfacial resistance arises because, from a kinetic point of view, condensation is the net result of vapor molecules condensing into liquid and liquid molecules evaporating into vapor. The fact that the two processes must be slightly out of balance (for net condensation to occur) results in a kinetic theory prediction of a temperature jump between the vapor and the liquid at the interface, and a somewhat lower liquid interfacial temperature than T_{sat}, and less driving force for heat transfer in the condensate film. Minkowycz and Sparrow [3] calculated the effects of interfacial resistance for steam-water condensation using the Schrage model and found it to depend on the accommodation coefficient (needed in Schrage model), temperature difference between the saturation and wall temperature, and the operating pressure. At normal pressure (101 kPa) and elevated pressures interfacial resistance was

negligible, and came into play only for lower pressures, small values of the accommodation coefficient, and small ΔT. However, it should be remarked that such calculations pertaining to the conditions and parameters of condensation of oxygen appear to be unavailable.

Minkowycz and Sparrow [3] also studied the effects of a non-condensable gas on the rate of condensation of a vapor. While the theory is developed in general, specific calculations are reported for the condensation of steam, with air as the non-condensable gas. The authors find that the condensation rate of steam is reduced by more than 50% when the mass fraction of air in the bulk vapor is as small as 0.5%, and by 85-90% when the mass fraction is 10%. The effect of the non-condensable is more severe at lower system pressure. The effect of ΔT on the reduction of the rate of condensation is complicated. At low mass fractions, the effect of the non-condensable decreases as ΔT is reduced but increases when the mass fraction is large. In general, vapor superheat tends to diminish the effect of non-condensables. It should be emphasized again that calculations with non-condensables pertaining to the condensation of oxygen appear to be unavailable.

Since the condensation heat transfer coefficients predicted in this study are quite large, even a significant reduction in it (similar to that predicted by Minkowycz and Sparrow) due the presence of non-condensables would still render the heat transfer coefficients to be large compared to that in the neon flow. While detailed calculations need to be performed, it appears that the liquefaction rate of oxygen is still limited by the capability of the cryocooler and not by the characteristics of condensation, even in the presence of non-condensables. However, for the same overall tank pressure, the partial pressure (and thus the saturation temperature) will decrease with fill level as the non-condensables accumulate in the tank. Thus, the temperature differential for heat transfer to the neon flow will decrease and the rate of condensation will be reduced. Indeed, testing with helium and nitrogen by Valenzuela [7] did show a decrease of liquefaction rate and heat transferred when helium is injected into the nitrogen tank.

5. Conclusions

A simplified model of broad area cooling of the outer surface of a cryogenic tank has been pursued to determine the rate of liquefaction of oxygen in it. It is shown that liquefaction is limited by the capability of the cryocooler used to remove heat from the tank via a neon loop acting as the coolant. The analysis shows that for gravity level on Earth, Moon or Mars, the physics of condensation within the tank has practically no influence on rate of heat transfer to the neon flow. Therefore, testing in Earth's gravity is likely adequate for validation and checking the performance of the liquefaction system.

References

[1] R. Zubrin, D. Daker, O. Gwynne, "Mars direct: a simple, robust, and cost-effective architecture for the space exploration initiative." In: 29th Aerospace Sciences Meeting, AIAA-91-329; 1991.

[2] W.L. Johnson, D.M. Hauser, D.W. Plachta, X-Y.J. Wang, B.F. Banker, P.S. Desai, J.R. Stephens, A.M. Swanger, "Comparison of oxygen liquefaction methods for use on the Martian surface," Cryogenics 90 (2018) 60-69.

[3] W.J. Minkowycz and E.M. Sparrow, "Condensation heat transfer in the presence of noncondensables, interfacial resistance, superheating, variable properties and diffusion," Int. J. Heat Mass Transfer, 9, 1125-1144, 1966.

[4] J. Gerstmann and P. Griffith, "Laminar film condensation on the underside of horizontal and inclined surfaces," Int. J. Heat Mass Transfer, 10, 567-580, 1967.

[5] A. Kashani, D. Hauser and P. Desai, "Propellant liquefaction modelling compared against liquefaction testing," 2020 IOP Conf. Ser.: Mater. Sci. Eng. 755 012006.

[6] E.M. Sparrow and E.R.G. Eckert, "Effects of Superheated Vapor and Noncondensable Gases on Laminar Film Condensation," AIChE Journal, 7(3), 473-477, 1961.

[7] J.G. Valenzuela, "Cryogenic In-Situ Liquefaction for Landers, “Brassboard” Liquefaction Testing Series," NASA TM-20210010564, 2021.